Spectral density of samarium sulfide

Christoph Lehner
Max-Planck-Institut für Physik komplexer Systeme, Nöthnitzer Straße 38, 01187 Dresden, Germany

Manuel Richter and Helmut Eschrig
Institut für Theoretische Physik, Technische Universität, 01062 Dresden, Germany

(Received 26 November 1997)

The spectral density of samarium sulfide is calculated using a multiband periodic Anderson model. The s, p, and d states are treated as band states within the local-density approximation. Realistic, local many-electron states of the $4f$ shell are taken into account. Using projection techniques a $4f$ occupation of 5.94 is found in the semiconducting phase. The calculated spectral density is in fair agreement with the measured photoemission and inverse photoemission spectra. To simulate the mixed-valent phase, the global hybridization strength between $4f$ and band states is empirically enhanced. The limits of a valence change controlled by the hybridization strength are discussed. [S0163-1829(98)01132-1]

I. INTRODUCTION

Samarium sulfide (SmS) has attracted much attention during the last 25 years (for an early theoretical review see Ref. 1). At 6.5 kbar and room temperature it shows an isostructural first-order phase transition from a black, semiconducting phase to a golden-yellow metallic phase[2] accompanied by a volume collapse of $\approx 13\%$. Photoemission spectra of semiconducting SmS (Ref. 3) show localized, atomiclike $4f^5$ final states at binding energies of 0.5–4.0 eV, which imply a dominating $4f^6$ ground state. Photoemission spectra of doped SmS simulating the collapsed phase[3] show again localized $4f^5$ final states and, energetically separated, $4f^4$ final states at higher binding energies that both clearly stem from the two $4f$ configurations $4f^5$ and $4f^6$ contributing to the ground state. Because of the strong localization of the $4f$ wave function, photoemission spectra of SmS look in first approximation like spectra for the isolated, free Sm^{2+} ion in the semiconducting case and like a static mixture of Sm^{2+} with Sm^{3+} ions in the mixed-valent case. Nevertheless, it is clear from the experimental equivalence of the Sm sites that the mixed-valent state in SmS is homogeneous, and this can only be provided by the hybridization of $4f$ states with delocalized band states of s, p, or d character.

A standard band-structure calculation in local-density approximation[4–7] (LDA) yields seven one-particle f bands with a total width of 0.7 eV at the Fermi energy. These states are twofold spin degenerate in the nonrelativistic case and twofold Kramers degenerate in the relativistic case. Attempts at a description beyond LDA have been published, where the common idea is to distinguish occupied and unoccupied $4f$-states. One possibility is to approximate the self-energy by introducing the Coulomb repulsion U as an additional parameter to the one-particle (LDA) equations for a quasiparticle band structure, as performed by López-Aguilar and Costa-Quintana.[8] This leads, after choosing the occupied $4f$-states, to a splitting between $4f$-states with $T_{2u}=\Gamma_{25}$ and $A_{2u}=\Gamma_2'$ symmetry (cubic point-group O_h) in the unoccupied part and those with $T_{1u}=\Gamma_{15}$ symmetry (six states) in the occupied part of the spectrum. In a different approach, Schumann *et al.*[9] took into account the self-interaction correction for the six relativistic states with total angular momentum $j=5/2$.

By construction, one-particle band-structure calculations for SmS (Refs. 4–9) do not address one-electron excitations that remain localized in the $4f$ shell and form local many-electron states. Such local states are seen by photospectroscopy,[10] which probes the one-particle excitation spectrum, i.e., the spectral density, within the sudden approximation[11] valid at high photon energies. To calculate the spectral density we adopted a generalized periodic Anderson model as the basis of the present work. It allows us to evaluate one-particle excitation spectra that reflect, in accordance with experiment, both the itinerant states and the local many-electron states. These latter states do weakly hybridize with the s-, p-, and d-like band states.

Several attempts have been made to calculate the excitation spectrum using simpler versions of the periodic Anderson model within a restricted space of localized $f^0/f^1/f^2$ states and only one band orbital.[12–18] Although much can be learned about the approximations used, a comparison to spectroscopy or an analysis of the valence of SmS is not possible in such a simplified frame. The emphasis in this work is on the high-energy side of the spectral density with particle and hole excitations of 0.3–10 eV. Special attention is given to atomiclike excitations inside the $4f$ shell and the changes that occur when they hybridize with delocalized band states.

After introducing our model Hamiltonian and the projection technique in Sec. II, we present the results in Sec. III and give finally our summary with conclusions in Sec. IV.

II. THEORY

A. Multiband model for SmS

A multiband Hubbard Hamiltonian naturally includes the interplay between localized and delocalized states through the on-site Coulomb repulsion and Hamiltonian matrix ele-

ments connecting different lattice sites. In the following, f states will be treated differently from s, p, and d states, where the latter are denoted as c states. Starting from localized f orbitals, we neglect f-f Hamiltonian and f-f overlap matrix elements for different lattice sites, as well as f-c overlap matrix elements,[19] but take into account f-c Hamiltonian, c-c overlap, and c-c Hamiltonian matrix elements. Although spin-orbit splitting is important it is neglected in the following because it only leads to a fine structure in the spectral density with splittings of order 0.1–0.5 eV for atomic $4f$ energy levels,[20] and splittings of about 0.7 eV for one-particle $4f$ bands,[6] a point not addressed in this paper. Now, the Hamiltonian consists of three parts:

$$H = H_{\mathrm{band}} + \sum_i H^f_{i,\mathrm{local}} + H_{\mathrm{mix}}. \tag{1}$$

H_{band} is the one-particle part for c states:

$$H_{\mathrm{band}} = \sum_{\mathbf{k},\sigma,\alpha,\beta} c^{\alpha\dagger}_{\mathbf{k},\sigma} [(\underline{\underline{O}}^{cc}_{\mathbf{k}})^{-1} \underline{\underline{H}}^{cc}_{\mathbf{k}} (\underline{\underline{O}}^{cc}_{\mathbf{k}})^{-1}]_{\alpha\beta} c^{\beta}_{\mathbf{k},\sigma}. \tag{2}$$

Here, $c^{\alpha(\dagger)}_{\mathbf{k},\sigma}$ are annihilation (creation) operators for electrons with lattice momentum $\mathbf{k}$ and spin σ in the c orbital with index α. The Hamiltonian and overlap matrices $H^{cc}_{\mathbf{k}}$ and $O^{cc}_{\mathbf{k}}$ are formed in the space of the c-basis states. The following anticommutation relation holds:

$$[c^{\alpha}_{\mathbf{k},\sigma}, c^{\beta\dagger}_{\mathbf{k},\sigma'}]_+ = \delta_{\sigma,\sigma'} (\underline{\underline{O}}^{cc}_{\mathbf{k}})_{\alpha\beta}. \tag{3}$$

$H^f_{i,\mathrm{local}}$ is diagonal in the local $4f$-shell eigenstates at site i:

$$H^f_{i,\mathrm{local}} = \sum_{n,A} E_{n,A} |i,n,A\rangle\langle i,n,A|. \tag{4}$$

Here, $|i,n,A\rangle$ denotes a local eigenstate of the $4f$ shell at site i, characterized by the occupation number n, certain additional quantum numbers A, and energy $E_{n,A}$. The quantum numbers A include total spin S and total angular momentum L of the $4f$ shell together with their projections M_L and M_S. Note that within our basis of $4f$-shell eigenstates the Coulomb repulsion at site i inside the $4f$ shell is included in $E_{n,A}$. At a given site, the following orthonormality and completeness relations hold:

$$\langle i,n,A|i,m,B\rangle = \delta_{mn}\delta_{AB}, \tag{5}$$

$$1_i = \sum_{n,A} |i,n,A\rangle\langle i,n,A|.$$

H_{mix} describes the f-c hybridization due to f-c Hamiltonian matrix elements:

$$\begin{aligned} H_{\mathrm{mix}} &= \sum_{\mathbf{k},\sigma,\alpha,\mu} c^{\alpha\dagger}_{\mathbf{k},\sigma} [(\underline{\underline{O}}^{cc}_{\mathbf{k}})^{-1} \underline{\underline{H}}^{cf}_{\mathbf{k}}]_{\alpha\mu} f^{\mu}_{\mathbf{k},\sigma} + \mathrm{H.c.} \\ &= \sum_{\mathbf{k},\sigma,\alpha,\mu,\Gamma} c^{\alpha\dagger}_{\mathbf{k},\sigma} [(\underline{\underline{O}}^{cc}_{\mathbf{k}})^{-1} \underline{\underline{H}}^{cf}_{\mathbf{k}}]_{\alpha\mu} M^{\sigma,\mu}_{\Gamma} X^{\Gamma}_{\mathbf{k}} + \mathrm{H.c.} \\ &= \sum_{\mathbf{k},\sigma,\alpha,\Gamma} c^{\alpha\dagger}_{\mathbf{k},\sigma} V^{\alpha,\Gamma}_{\mathbf{k},\sigma} X^{\Gamma}_{\mathbf{k}} + \mathrm{H.c.} \end{aligned} \tag{6}$$

In the first line of Eq. (6), $f^{\mu}_{\mathbf{k},\sigma}$ annihilates an electron in the Bloch state of $4f$ orbitals μ with spin σ. In the second line of Eq. (6), a basis transformation from Fermi operators $f^{\mu}_{\mathbf{k},\sigma}$ to Hubbard operators[21]

$$X^{\Gamma}_{\mathbf{k}} \overset{\mathrm{def}}{=} \frac{1}{N} \sum_i e^{-i\mathbf{k}\cdot\mathbf{R}_i} X^{\Gamma}_i = \frac{1}{N} \sum_i e^{-i\mathbf{k}\cdot\mathbf{R}_i} |i,n-1,B\rangle\langle i,n,A| \tag{7}$$

has been performed:

$$\begin{aligned} f^{\mu}_{i,\sigma} &= 1_i f^{\mu}_{i,\sigma} 1_i \\ &= \sum_{n,A,B} \langle i,n-1,B|f^{\mu}_{i,\sigma}|i,n,A\rangle |i,n-1,B\rangle\langle i,n,A| \\ &\overset{\mathrm{def}}{=} \sum_{\Gamma} M^{\sigma,\mu}_{\Gamma} X^{\Gamma}_i. \end{aligned} \tag{8}$$

The Hubbard operators X^{Γ}_i make transitions

$$\Gamma = (n,A;n-1,B) \tag{9}$$

from local eigenstate $|i,n,A\rangle$ to local eigenstate $|i,n-1,B\rangle$. The matrix elements $M^{\sigma,\mu}_{\Gamma}$ are site independent and can be reduced using the point-group symmetries of the rare-earth site. The symmetry-reduced matrix elements in spherical symmetry were first calculated by Racah[22] and can be chosen as real numbers (see Appendix A). The $M^{\sigma,\mu}_{\Gamma}$ fulfill the following sum rules:

$$\begin{aligned} \sum_{\sigma,\mu,B} M^{\sigma,\mu}_{n,A;n-1,B} M^{\sigma,\mu}_{n,A';n-1,B} &= \delta_{AA'} n, \\ \sum_{\sigma,\mu,A} M^{\sigma,\mu}_{n,A;n-1,B} M^{\sigma,\mu}_{n,A;n-1,B'} &= [14-(n-1)]\delta_{BB'}, \end{aligned} \tag{10}$$

which is a consequence of $|i,n,A\rangle$ being an eigenstate of the number operator $\Sigma_{\sigma,\mu} f^{\dagger}_{i,\sigma} f_{i,\sigma}$. In the third line of Eq. (6) we have used the additional abbreviation:

$$\begin{aligned} V^{\alpha,\Gamma}_{\mathbf{k},\sigma} &= \sum_{\mu} [(\underline{\underline{O}}^{cc}_{\mathbf{k}})^{-1} \underline{\underline{H}}^{cf}_{\mathbf{k}} (\underline{\underline{O}}^{ff}_{\mathbf{k}})^{-1}]_{\alpha\mu} M^{\sigma,\mu}_{\Gamma} \\ &= \sum_{\mu} [(\underline{\underline{O}}^{cc}_{\mathbf{k}})^{-1} \underline{\underline{H}}^{cf}_{\mathbf{k}}]_{\alpha\mu} M^{\sigma,\mu}_{\Gamma}. \end{aligned} \tag{11}$$

The advantage of expressing all f operators in terms of Hubbard operators is that the physically important limit of non-

hybridizing f and c states can be treated accurately (with neglecting $\underline{\underline{O}}^{cf}$) and the hybridization as a weak perturbation.

B. Projection technique

In this paper our main interest is the spectral density $\rho_{\mathbf{k}}^{f/c}(\omega)$ for c and f states:

$$\rho_{\mathbf{k}}^{f/c}(\omega)=\frac{i}{2\pi}\lim_{\delta\searrow 0}[G_{\mathbf{k}}^{f/c}(\omega+i\delta)-G_{\mathbf{k}}^{f/c}(\omega-i\delta)], \quad (12)$$

which can be obtained from the corresponding one-particle Green function $G_{\mathbf{k}}^{f/c}(\omega)$,

$$G_{\mathbf{k}}^{f}(\omega)=\sum_{\sigma,\mu}\langle\langle f_{\mathbf{k},\sigma}^{\mu};f_{\mathbf{k},\sigma}^{\mu\dagger}\rangle\rangle_{\omega}, \quad (13)$$

$$G_{\mathbf{k}}^{c}(\omega)=\sum_{\sigma,\alpha,\beta,\gamma}\langle\langle[(\underline{\underline{O}}_{\mathbf{k}}^{cc})^{-1/2}]_{\alpha\beta}c_{\mathbf{k},\sigma}^{\beta};c_{\mathbf{k},\sigma}^{\gamma\dagger}[(\underline{\underline{O}}_{\mathbf{k}}^{cc})^{-1/2}]_{\gamma\alpha}\rangle\rangle_{\omega}.$$

Here, the energy representation $\langle\langle D;B\rangle\rangle_{\omega}$ for annihilation operators D and B refers to a retarded Green function:

$$\langle\langle D;B^{\dagger}\rangle\rangle_{\omega}\overset{\text{def}}{=}-i\int_{-\infty}^{\infty}dt\,\theta(t)e^{i\omega t}\langle[D(t),B(0)^{\dagger}]_{+}\rangle, \quad (14)$$

where the average $\langle\cdots\rangle$ in general refers to the thermodynamic average at temperature T. Throughout this work it is used for the ground-state expectation value, $T=0$. The one-particle f Green function can be obtained using Eq. (8) from the Hubbard Green functions:

$$G_{\mathbf{k}}^{f}(\omega)=\sum_{\Gamma}\left(\langle\langle X_{\mathbf{k}}^{\Gamma};X_{\mathbf{k}}^{\Gamma\dagger}\rangle\rangle\sum_{\sigma,\mu}(M_{\Gamma}^{\sigma,\mu})^{2}+\sum_{\Delta\neq\Gamma}\mathrm{Re}\langle\langle X_{\mathbf{k}}^{\Gamma};X_{\mathbf{k}}^{\Delta\dagger}\rangle\rangle\sum_{\sigma,\mu}M_{\Gamma}^{\sigma,\mu}M_{\Delta}^{\sigma,\mu}\right). \quad (15)$$

Evaluating the one-particle Green function, one makes use of the equation of motion for Heisenberg operators:

$$\omega\langle\langle D;B^{\dagger}\rangle\rangle_{\omega}=\langle[D,B^{\dagger}]_{+}\rangle+\langle\langle[D,H]_{-};B^{\dagger}\rangle\rangle_{\omega}. \quad (16)$$

The projection or partitioning technique[23,24] restricts the dynamics to a certain subset D_i $(i=1,\ldots,n;\ D_1\equiv D)$ of operators, which are considered as relevant, neglecting the irrelevant part:[25]

$$[D_i,H]_{-}\approx\sum_{l=1}^{n}D_lK_{li}. \quad (17)$$

Here, K_{li} are in general complex numbers to be determined. With the definition of the frequency matrix $\underline{\underline{F}}$ and the susceptibility matrix $\underline{\underline{\chi}}$:

$$(\underline{\underline{\chi}})_{ij}\overset{\text{def}}{=}\langle[D_i^{\dagger},D_j]_{+}\rangle, \quad (18)$$

$$(\underline{\underline{F}})_{ij}\overset{\text{def}}{=}\langle[D_i^{\dagger},[H,D_j]_{-}]_{+}\rangle, \quad (19)$$

the Green function matrix $(\underline{\underline{G}})_{ij}=\langle\langle D_j;D_i^{\dagger}\rangle\rangle$ can be written as

$$\underline{\underline{G}}(\omega)=\underline{\underline{\chi}}(\omega\ \underline{\underline{\chi}}+\underline{\underline{F}})^{-1}\underline{\underline{\chi}}, \quad (20)$$

and the numbers $K_{ij}=(\underline{\underline{K}})_{ij}$ become

$$\underline{\underline{K}}=-\underline{\underline{\chi}}^{-1}\underline{\underline{F}}. \quad (21)$$

Equation (20) can be solved through diagonalization. The matrix elements $\underline{\underline{F}}$ and $\underline{\underline{\chi}}$ contain expectation values $\langle D_i^{\dagger}D_j\rangle$ to be determined from corresponding Green functions through the spectral theorem until self-consistency is reached:

$$\langle D_i^{\dagger}D_j\rangle=\frac{i}{2\pi}\lim_{\delta\searrow 0}\int_{-\infty}^{E_F}d\omega[G_{ij}(\omega+i\delta)-G_{ij}(\omega-i\delta)]. \quad (22)$$

Here, E_F is the Fermi energy.

A minimal choice of the relevant set of operators in Eq. (17) should contain at least the unhybridized limit of model (1) exactly and this means the choice of two classes of operators:

$$D_{\mathbf{k}}^{\Gamma}=\sum_{i}e^{-i\mathbf{k}\cdot\mathbf{R}_i}|i,n-1,B\rangle\langle i,n,A|, \quad (23)$$

$$D_{\mathbf{k},\sigma}^{\alpha}=c_{\mathbf{k},\sigma}^{\alpha}. \quad (24)$$

The resulting matrices $\underline{\underline{F}}$ and $\underline{\underline{\chi}}$ in these variables are listed in Appendix B.

The next dynamical variables $D_{\mathbf{k}',\alpha,\sigma}^{\mathbf{k},n,A,A'}$ to be taken into account involve the annihilation of a band electron accompanied by a simultaneous fluctuation in the $4f$ shell with fixed occupation number:

$$D_{\mathbf{k}',\alpha,\sigma}^{\mathbf{k},n,A,A'}=\sum_{j}e^{i(\mathbf{k}-\mathbf{k}')\mathbf{R}_j}|j,n,A'\rangle\langle j,n,A|c_{\mathbf{k}'\sigma}^{\alpha}. \quad (25)$$

We neglect the influence of these higher-order processes on the dynamics of one particle in Eq. (17).

Examples demonstrating the use and merits of the projection technique can be found in the textbook by Fulde.[26] Further, applications of this technique to multiband Hubbard models for high-T_c superconductors and $3d$ metals were presented in the papers by Unger and co-workers.[27–29]

Generally speaking, the projection technique allows for a mapping of the spectral density to dynamical variables. In this way, a physical transparent interpretation of any given excitation becomes possible by considering the algebraic expressions of the dynamical variables. The relation of the projection technique to a moment expansion of the spectral density[30] reproduces expecially well the high-energy region of the spectra. On the other hand, an accurate picture of the low-energy region of the spectral density involving an infinite number of degrees of freedom is not easily obtained through the choice of a finite set of relevant dynamical variables. However, the effect of dynamical variables not in-

cluded in the relevant set, Eq. (17) on the dynamics of one electron could be captured by the memory matrix and calculated approximately.[26]

C. Quasidegeneracies

Without spin-orbit coupling the eigenstates of an isolated ion for given occupation number are LS terms that are in general highly degenerate with respect to quantum numbers M_S and M_L for a given quantization axis. The spectral f density of the model (1) in the case of nonhybridizing f-c states is diagonal in the space of Hubbard operators. It then consists of dispersionless, degenerate lines whose weights are determined by the squared matrix elements $(M_\Gamma^{\sigma,\mu})^2$ according to Eq. (15) and the ground-state composition of $4f$-shell states. A uniform ground state for isolated $4f$ shells on a lattice, for example, consists of only one $4f$ state.

In the case of nonhybridizing $4f$ states, it is possible to sum the dynamical variables of Eq. (23) over degeneracies of local states from the beginning, which reduces the dimension of the matrices considerably. In the case of a weak hybridization, the degenerate excitations in the spectral f density are expected to split weakly and become **k** dependent. It is desirable to describe this narrow collection of lines by one effective dynamical variable

$$\Gamma_{\text{eff}} \overset{\text{def}}{=} \sum_{\text{degeneracies}} \Gamma, \tag{26}$$

which is a further simplification on top of the approximate treatment of the hybridization in the selection of dynamical variables. The sum over degeneracies in Eq. (26) is over all M_L, M_S quantum numbers that are involved in the transition Γ. Note that this simplification keeps the size of the matrices involved in Eq. (20) tractable.

Summing the matrix elements $(M_\Gamma^{\sigma,\mu})^2$ over single ion degeneracies results in an effective matrix element $M_{\Gamma_{\text{eff}}}$:

$$M^2_{\Gamma_{\text{eff}}} \overset{\text{def}}{=} \frac{1}{N_{\text{deg}}} \sum_{\text{degeneracies}} (M_\Gamma^{\sigma,\mu})^2. \tag{27}$$

N_{deg} is a normalization constant and counts the number of terms in the sum. It turns out that $M^2_{\Gamma_{\text{eff}}}$ is σ,μ *independent* and essentially a symmetry-reduced matrix element. (In Appendix A all symmetry-reduced matrix elements used in this work are listed.) However, the coupling $\underline{\underline{H}}_{\mathbf{k}}^{cf}$ of one-particle f orbitals to c states is of course *not* independent of the f orbital index μ. Therefore, a simple summation over μ in Eq. (11) might violate the crystal symmetry. We avoid this by restricting ourselves to an f orbital, which is a one-dimensional representation of the real-space point group of the Bravais lattice under consideration. In the cubic point group of Sm in SmS, the f_{xyz} orbital plays this role and replaces all seven f orbitals in our treatment. Equation (11) is replaced by

$$(V_{\mathbf{k}}^{\alpha,\Gamma})^{\text{eff}} = 7[(\underline{\underline{O}}_{\mathbf{k}}^{cc})^{-1} \underline{\underline{H}}_{\mathbf{k}}^{cf}]_{\alpha,\mu=xyz} M_{\Gamma_{\text{eff}}}. \tag{28}$$

The introduction of effective dynamical variables in Eq. (26) together with effective matrix elements in Eq. (27) enforces two further approximations. The effective matrix elements in Eq. (27) cannot reproduce off-diagonal sum rules [$A \neq A'$ or $B \neq B'$ in Eq. (10)]. Therefore, only diagonal Hubbard Green functions in Eq. (15) are taken into account:

$$\langle\langle f_{\mathbf{k},\sigma}^{\mu}; f_{\mathbf{k},\sigma}^{\mu\dagger}\rangle\rangle \approx \sum_{\Gamma} \langle\langle X_{\mathbf{k}}^{\Gamma}; X_{\mathbf{k}}^{\Gamma\dagger}\rangle\rangle (M_\Gamma^{\sigma,\mu})^2. \tag{29}$$

Consequently, it is impossible to calculate off-diagonal matrix elements between $4f$-shell transitions in the susceptibility matrix (18), and they are neglected:

$$\langle [(X_{\mathbf{k}}^{\Delta})^\dagger, X_{\mathbf{k}}^{\Gamma}]_+ \rangle \approx \delta_{\Gamma\Delta} \langle [(X_{\mathbf{k}}^{\Gamma})^\dagger, X_{\mathbf{k}}^{\Gamma}]_+ \rangle. \tag{30}$$

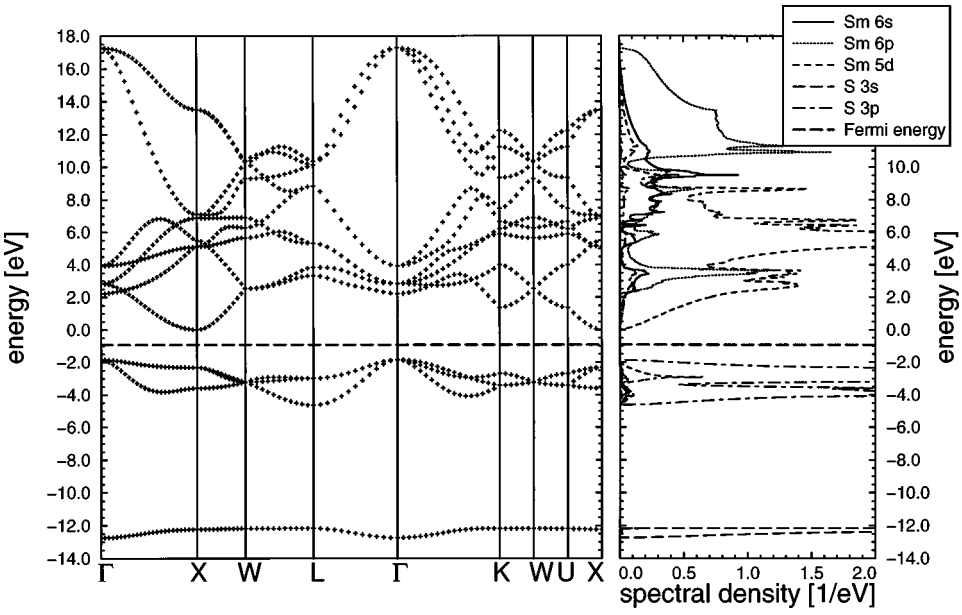

FIG. 1. Band structure (left part) and spectral density (right part) of delocalized band states. Six $4f$ electrons are frozen in the core. The reference point of zero energy is chosen as the bottom of the conduction band of c states.

III. RESULTS

A. Realistic parameters

The Hamiltonian and overlap matrices for band states c are calculated in LDA to density-functional theory using an optimized linear combination of atomic orbitals (LCAO) band-structure code.[31] Sm $6s$, $6p$, and $5d$ states as well as S $3s$ and $3p$ states are treated as valence states. Six $4f$ electrons were put in the core. In this way the f-c hybridization was completely switched off while calculating band states. The remaining interaction between f and band states in this type of calculation is indirect via electrostatic (Hartree) and exchange and correlation potential and determines the radial dependence of the $4f$ wave function. The lattice constant of 5.97 Å for the black phase was taken to be representative also for the golden phase as far as the band states are concerned. The one-particle LDA-Hamiltonian matrix elements between f and c states in the self-consistent charge distribution of c states are determined and later used in expression (28). The resulting band structure of c states is shown in Fig. 1.

We now turn to the choice of relevant local states. A ground state with two coexisting configurations f^n and f^{n-1} implies final states in the spectral density, which range from f^{n-2} to f^{n+1}, if one electron is removed or added. Therefore, we take into account all 22 excited states of f^4-f^7, which can be reached by removing or adding an electron from/to the atomic ground states of f^5 or f^6. This gives 24 LS terms as local eigenstates [see Eq. (5) and Table I for a complete listing]. The sum over their ground state contributions is assumed to be one. Together with the transition between the two ground states of f^5 and f^6, one obtains 23 local transitions (see Table II), which enter as dynamical variables in Eq. (23).

The relative energies for the local many-electron states of the $4f$ shell with fixed occupation number, the LS terms, are taken from experimental optical spectra of the free, trivalent rare earth ions Pm^{3+}, Sm^{3+}, Eu^{3+}, and Gd^{3+} in the solution.[20] These energies in the experimental spectra are contracted or expanded by 10% in order to account for each nuclear charge less or larger, respectively, than that of samarium.[10] The experimental LSJ energies corresponding to the same LS term are averaged according to their J multiplicity in order to get an average LS energy. All average LS energies used in this work are listed in Table I. The relative energy differences between ground states of different occupation cannot be taken from single ion values, since screening by conduction electrons is present in the solid. They have to be adjusted to photoemission[3] and inverse photoemission,[33] with respect to a given band reference energy. The optimal parameter choice is shown in Table III.

For the description of the mixed-valent phase, the LDA hybridization strength is scaled with a global, empirical parameter α to account for the increase of the f-c hybridization matrix elements during lattice contraction from the black to the golden phase. These matrix elements would increase by approximately a factor $\alpha=1.2$ due to the volume collapse. This factor is too small for a reasonable valence change and visible changes of the spectral density. To demonstrate the qualitative effect of a volume change in our model more clearly, we chose arbitrarily a factor $\alpha=2$ in the following for the metallic, mixed-valent phase of SmS. As a justification for this choice one should keep in mind the *a priori* approximative character of the model Hamiltonian and the additional approximations used for the determination of the Green function which might be not enough sensitive for small changes of matrix elements caused by the lattice contraction. Note that all other parameters of the model Hamiltonian remain fixed and the same for both phases. We do not attempt to explain the thermodynamics of the first order phase transition in SmS.

TABLE I. LS-term energies in eV, with respect to the ground state of the f^n configuration. The term energies for f^4, f^5, f^6, and f^7 originate from Pm^{3+}, Sm^{3+}, Eu^{3+}, and Gd^{3+} ultraviolet f-f absorption data (Ref. 20). γ is the contraction or expansion factor to be applied as mentioned in the text. Some of the LS terms have been classified by an additional number according to the notation used in Ref. 32. Note that the state $f^6(^5H1)$ cannot be reached from the ground state due to a zero matrix element with $f^5(^6H)$ and is left out here. Further, terms with the same energy are not distinguished in our approach and appear on the same line.

Term	Energy (eV)	γ
$f^4(^5I)$	0.00	1.11
$f^4(^5F)$	1.31	1.11
$f^4(^5G)$	2.10	1.11
$f^4(^5D)$	3.36	1.11
$f^5(^6H)$	0.00	1.00
$f^5(^6F)$	0.58	1.00
$f^5(^6P)$	2.67	1.00
$f^6(^7F)$	0.00	0.90
$f^6(^5D3)$	2.34	0.90
$f^6(^5G3)$	2.62	0.90
$f^6(^5L)$	2.72	0.90
$f^6(^5H2)$	3.14	0.90
$f^6(^5F1)$, $f^6(^5F2)$	3.40	0.90
$f^6(^5I1)$, $f^6(^5I2)$	3.53	0.90
$f^6(^5K)$	3.94	0.90
$f^6(^5D1)$, $f^6(^5D2)$	4.14	0.90
$f^6(^5G1)$, $f^6(^5G2)$	4.13	0.90
$f^7(^8S)$	0.00	0.81
$f^7(^6P)$	4.05	0.81
$f^7(^6I)$	4.52	0.81
$f^7(^6D)$	5.02	0.81
$f^7(^6G)$	6.22	0.81
$f^7(^6F)$	6.76	0.81
$f^7(^6H)$	7.27	0.81

B. Spectral density

The spectral density for isolated $4f$ shells shows dispersionless lines with weights different from unity in contrast to simple one-particle states. In the case of an empty $4f$ shell for example, the weight corresponding to the transition $f^0 \rightarrow f^1$ in the unoccupied part of the spectrum is 14 and 0 in the occupied part of the spectrum. In the unhybridized limit our model shows a pure $f^6(^7F)$ ground state. This is due to the fact that the lowest-lying occupied f excitation is 0.7 eV below the bottom of the conduction band for c states, as seen

TABLE II. Reduced matrix elements of the f operator between many-electron states of the $4f$ shell. They have been calculated first by Racah (Ref. 22). Degenerate transitions (on the same line) enter as the same dynamical variable in our approach.

Transition	Matrix element	Value
$f^7 \rightarrow f^6$	$[f^6(^7F)\|f\|f^7(^8S)]$	$\sqrt{56}$
	$[f^6(^7F)\|f\|f^7(^6I)]$	$-\sqrt{91}$
	$[f^6(^7F)\|f\|f^7(^6H)]$	$-\sqrt{77}$
	$[f^6(^7F)\|f\|f^7(^6G)]$	$-\sqrt{63}$
	$[f^6(^7F)\|f\|f^7(^6F)]$	$-\sqrt{49}$
	$[f^6(^7F)\|f\|f^7(^6D)]$	$-\sqrt{35}$
	$[f^6(^7F)\|f\|f^7(^6P)]$	$-\sqrt{21}$
$f^6 \rightarrow f^5$	$[f^5(^6H)\|f\|f^6(^7F)]$	$\sqrt{154}$
	$[f^5(^6F)\|f\|f^6(^7F)]$	$7\sqrt{2}$
	$[f^5(^6P)\|f\|f^6(^7F)]$	$\sqrt{42}$
	$[f^5(^6H)\|f\|f^6(^5L)]$	$\sqrt{102}$
	$[f^5(^6H)\|f\|f^6(^5K)]$	$\sqrt{90}$
	$[f^5(^6H)\|f\|f^6(^5I1)]$, $[f^5(^6H)\|f\|f^6(^5I2)]$	$\sqrt{\frac{182}{3}}$, $\sqrt{\frac{52}{3}}$
	$(f^5(^6H)\|f\|f^6(^5H1)]$	0
	$[f^5(^6H)\|f\|f^6(^5H2)]$	$\sqrt{66}$
	$[f^5(^6H)\|f\|f^6(^5G1)]$, $[f^5(^6H)\|f\|f^6(^5G2)]$	$-\sqrt{\frac{195}{7}}$, $-\sqrt{\frac{390}{3}}$
	$[f^5(^6H)\|f\|f^6(^5G3)]$	$\sqrt{\frac{891}{7}}$
	$[f^5(^6H)\|f\|f^6(^5F1)]$, $[f^5(^6H)\|f\|f^6(^5F2)]$	$\sqrt{11}$, 3
	$[f^5(^6H)\|f\|f^6(^5D1)]$, $[f^5(^6H)\|f\|f^6(^5D2)]$	$-\sqrt{\frac{220}{21}}$, $-\sqrt{\frac{440}{147}}$
	$[f^5(^6H)\|f\|f^6(^5D3)]$	$\frac{9}{7}\sqrt{10}$
$f^5 \rightarrow f^4$	$[f^4(^5I)\|f\|f^5(^6H)]$	$\sqrt{182}$
	$[f^4(^5G)\|f\|f^5(^6H)]$	$-\sqrt{\frac{585}{7}}$
	$[f^4(^5F)\|f\|f^5(^6H)]$	$-\sqrt{33}$
	$[f^4(^5D)\|f\|f^5(^6H)]$	$-\sqrt{\frac{220}{7}}$

in Table III. The three transitions with $f^6(^7F)$ as initial state, $^7F \rightarrow {}^6H$, $^7F \rightarrow {}^6F$, and $^7F \rightarrow {}^6P$ lie in the occupied part of the spectrum, and have the noninteger weights of squared reduced matrix elements (see Table II), which sum up to exactly six. The unoccupied part of the spectrum consists of seven transitions $f^6(^7F) \rightarrow f^7$ according to Table II with an integrated weight of eight.

It follows from the definition (13) of the f spectral density that its normalization is 14 also in the general case with hybridization. Our choice of dynamical variables shows discrete poles at each $\mathbf{k}$ point. In general, their f weights differ from their unhybridized values due to a change of the ground-state composition. Moreover, the excitations with dominant f character now show a dispersion due to hybridization. Figure 2 shows the partial spectral densities for the semiconducting and mixed-valent phase. The $4f$ occupation is determined by integration giving 5.94 in the semiconducting and 5.78 in the mixed-valent phase (see the next subsection). The main change in the spectral density when going from the semiconducting to the mixed-valent phase is the occurrence of f^4 final states at higher binding energies between -8.0 and -12.5 eV and more pronounced f^6 final-state multiplets in the unoccupied part at energies between 2 and 4 eV.

Finally, a direct comparison of experimental photoemission[3] and inverse photoemission spectra[33] with the calculated partial f density is made in Fig. 3. For the semiconducting phase of SmS the theoretical Fermi energy of a pure sample should lie very close to the lower conduction-band edge due to the strongly different effective masses of conduction states with Sm $5d$ character and valence states with Sm $4f$ character. Without any major error, we put the Fermi energy in the theoretical calculations exactly at the lower conduction-band edge. Note that the experimentally determined chemical potential of a semiconductor can be easily shifted by defects or additional charges on the sample and is moreover influenced by the surface sensitivity of photoemission in general. In addition, the X-ray photoemission

TABLE III. Adjustment of energy differences for different $4f$ occupations. The bottom of the conduction band is taken to be the Fermi level.

Ground-state energy difference	(eV)
$E_0(f^7)-E_0(f^6)$	3.0
$E_0(f^6)-E_0(f^5)$	-0.7
$E_0(f^5)-E_0(f^4)$	-7.7

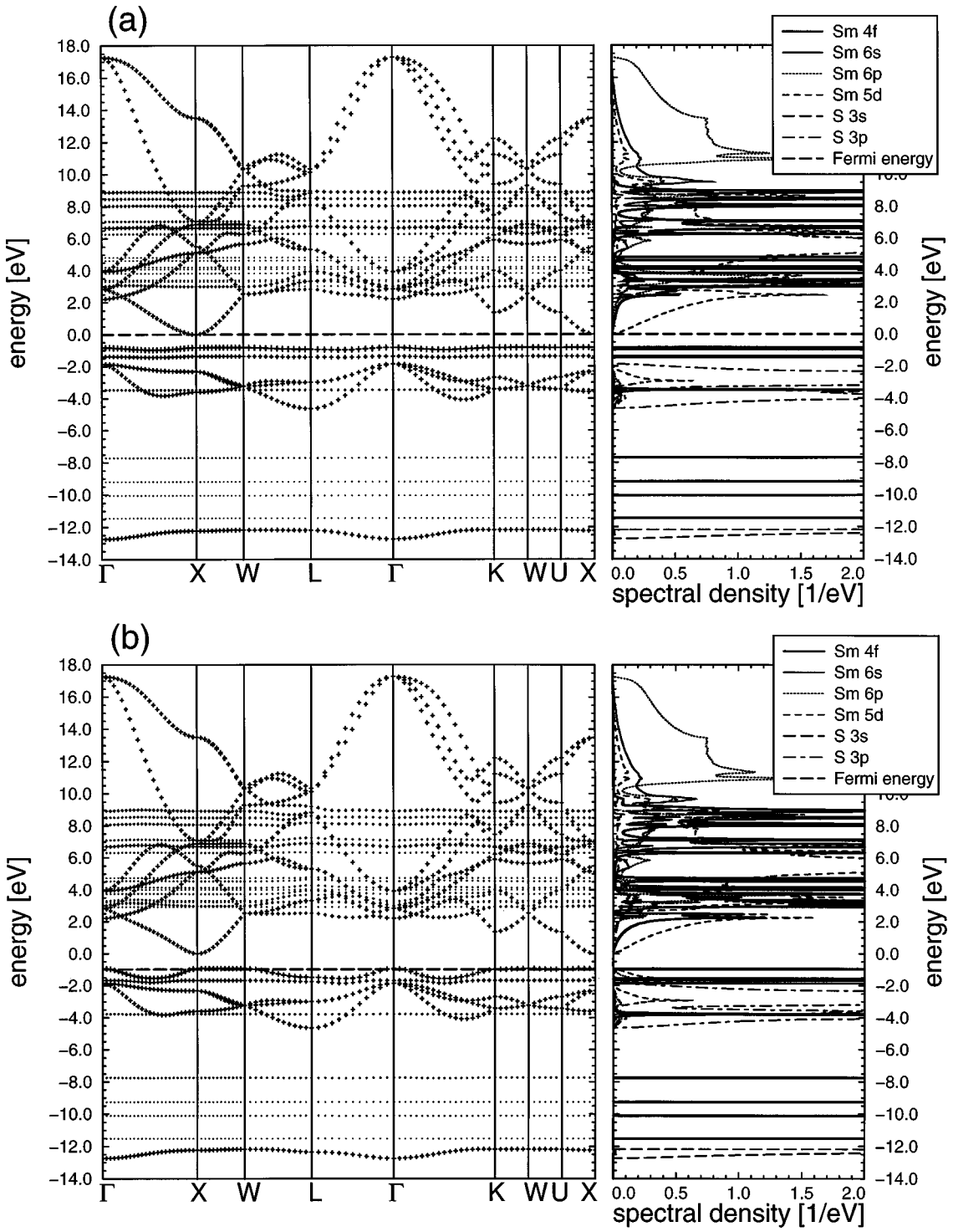

FIG. 2. **k**-resolved spectral densities for the semiconducting (a) and the mixed-valent phase (b), in the left part of the figures. The width of the crosses is proportional to the total pole strength. Note that poles with weight <0.065 in left part of (a) at energies between -10 and -12 eV can graphically not be correctly resolved and are overemphasized. **k**-integrated spectral densities are given in the right part of the figures. The reference point of zero energy is as in Fig. 1 and temperature is $T=0$ K.

spectroscopy (XPS) and bremsstrahlung isochromat spectroscopy (BIS) experiments were not done with the same sample and hence the coincidence of the two individual chemical potentials is not guaranteed. Despite these uncertainties, we assume sufficient accuracy of both experimental chemical potentials. It should be mentioned that our theory has not enough predictive power for absolute values of binding energies because the position of the lowest-lying f excitation in the semiconducting phase $^7F \rightarrow {}^6H$ is approximately given by a fit parameter, namely, the related energy difference $E_0(f^6)-E_0(f^5)$ (see Table III). This fit parameter determines essentially the band gap for the photoemission ex-

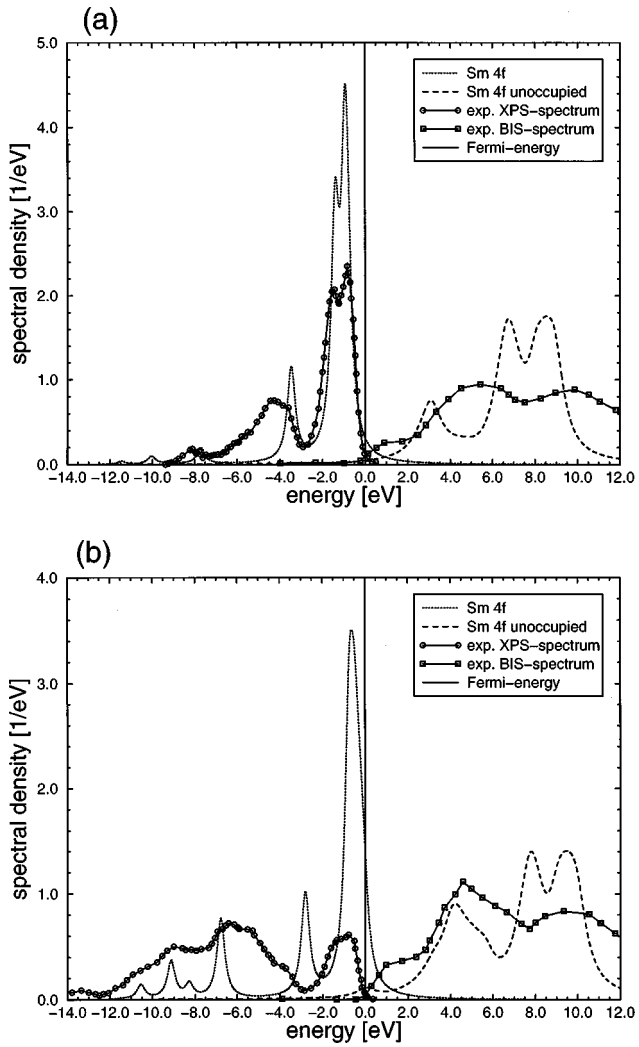

FIG. 3. Spectral f density compared to experimental XPS spectra (Ref. 3) and BIS spectra (Ref. 33). The experimental spectra have been normalized to the calculated ones, for occupied and unoccupied states separately. The calculated spectra have been broadened by a Lorentzian of 0.2 eV full width at half maximum for the occupied states and 0.5 eV for the unoccupied states. Temperature is $T=0$ K. (a) Semiconducting SmS, (b) collapsed (mixed-valent) SmS. Experimentally, the mixed-valent phase was prepared either by doping with thorium (XPS spectrum, Ref. 3) or as inhomogenous mixed-valent phase by partial oxidation (BIS spectrum, Ref. 33).

periment, which is different from the optical gap due to fast time scale (10^{-16} s) of the photoemission experiment compared to the slow time scale (10^{-10} s) of an optical experiment.

We compare the partial f density with experimental data for high photon energies ($\approx$1500 eV), where the cross section of $4f$ states is a factor of 10 larger than the cross section of other states. The calculated spectra are in fair agreement for the occupied region, and in reasonable agreement in the unoccupied region. One should note that the collapsed phase of SmS was prepared with thorium doping rather than by applying pressure in the photoemission experiment.[3] In the case of inverse photoemission,[33] the comparison remains only qualitative for the collapsed phase, because in the experiment an *inhomogenous* mixed valent phase consisting of SmS and Sm_2O_3 was prepared by partial oxidation. In particular, the amount of divalent and trivalent Sm sites contributing to the spectrum was unknown. On the theoretical side, the itinerant character of f states resulting from nonzero f-f hopping matrix elements that are neglected in this calculation should play a more important role for the unoccupied part of the spectrum with the more extended $N+1$ final-state wave functions.

C. Ground state and final states

The self-consistent ground state can be analyzed in terms of occupation numbers and LS-term contributions. The ground-state weight $p_{n,A}$ of the state $|n,A\rangle$ (i.e., the LS terms) for a ground state (GS) that does not break translation symmetry of the lattice,

$$p_{n,A} \overset{\text{def}}{=} \langle \mathrm{GS}|i,n,A\rangle\langle i,n,A|\mathrm{GS}\rangle, \tag{31}$$

can be easily related to the $4f$ occupation:

$$\langle n_f\rangle \overset{\text{def}}{=} \sum_{\mathbf{k},\sigma,\mu} \langle f^{\mu\dagger}_{\mathbf{k},\sigma} f^{\mu}_{\mathbf{k},\sigma}\rangle$$

$$= \langle \mathrm{GS}|n_f 1_i|\mathrm{GS}\rangle = \sum_{n,A} \langle \mathrm{GS}|n_f|i,n,A\rangle\langle i,n,A|\mathrm{GS}\rangle$$

$$= \sum_{n,A} n p_{n,A}\,. \tag{32}$$

The $4f$ occupation is therefore simply determined by taking the probability of finding an (initial) state $|n,A\rangle$ in the ground state, multiplied by the number of possibilities to remove an electron out of this configuration (that is, the number n of electrons present), and finally summing over all possible initial states. Note, that expression (32) holds for the fully hybridized ground state. Similarly, for the integrated unoccupied part $I^{\mathrm{unocc}}=14-n_f$ of the spectral density, one finds

$$I^{\mathrm{unocc}} = \sum_{n,A} (14-n) p_{n,A}\,. \tag{33}$$

Table IV shows the ground-state composition in terms of states $|n,A\rangle$ and occupation numbers.

The contributions of spectral weight to the integrated quantity n_f can be analyzed further in terms of local transitions. We define, in analogy to Eq. (15), a partial f Green function G^f_Γ associated with the local transition Γ:

$$G^f_\Gamma(\omega) = \frac{1}{N}\sum_{\mathbf{k}} \Bigg(\langle\langle X^{\Gamma}_{\mathbf{k}}; X^{\Gamma\dagger}_{\mathbf{k}}\rangle\rangle \sum_{\sigma,\mu} (M^{\sigma,\mu}_{\Gamma})^2 + \sum_{\Delta\neq\Gamma} \mathrm{Re}\langle\langle X^{\Gamma}_{\mathbf{k}}; X^{\Delta\dagger}_{\mathbf{k}}\rangle\rangle \sum_{\sigma,\mu} M^{\sigma,\mu}_{\Gamma} M^{\sigma,\mu}_{\Delta} \Bigg). \tag{34}$$

TABLE IV. Analysis of the semiconducting and the mixed-valent phase.

		Semiconducting	Mixed valent
$4f$-shell	$\mathrm{Sm}f^4$	<0.001	<0.001
weight $p_{n,A}$	$\mathrm{Sm}f^5(^6H)$	0.051	0.192
	$\mathrm{Sm}f^5(^6F)$	0.008	0.025
	$\mathrm{Sm}f^5(^6P)$	<0.001	0.003
	$\mathrm{Sm}f^6(^7F)$	0.939	0.771
	$\mathrm{Sm}f^6$ (other)	<0.001	0.007
	$\mathrm{Sm}f^4$ (sum)	<0.001	<0.001
	$\mathrm{Sm}f^5$ (sum)	0.059	0.220
	$\mathrm{Sm}f^6$ (sum)	0.940	0.778
	$\mathrm{Sm}f^7$ (sum)	<0.001	0.003
	Sm (sum)	1.000	1.000
Occupation	Sm $4f$	5.940	5.783
per	Sm $5d$	0.339	0.451
unit cell	Sm $6s$	0.056	0.056
	Sm $6p$	0.079	0.114
	S $3s$	1.994	1.994
	S $3p$	5.603	5.607
	total charge	14.000	14.000

For the following consideration we do not make use of approximation (29). Integrating the spectral density ρ^f_Γ associated with G^f_Γ up to the Fermi energy, the f occupation number can be alternatively expressed as

$$
\begin{aligned}
n_f &= \sum_\Gamma \Bigg(\sum_{\mathbf{k}} \langle X^{\Gamma\dagger}_{\mathbf{k}} X^\Gamma_{\mathbf{k}} \rangle \sum_{\sigma,\mu} (M^{\sigma,\mu}_\Gamma)^2 \\
&\quad + \sum_{\Delta\neq\Gamma} \mathrm{Re} \sum_{\mathbf{k}} \langle X^{\Delta\dagger}_{\mathbf{k}} X^\Gamma_{\mathbf{k}} \rangle \sum_{\sigma,\mu} M^{\sigma,\mu}_\Gamma M^{\sigma,\mu}_\Delta \Bigg) \\
&= \sum_{n,A} \Bigg(\langle \mathrm{GS}|i,n,A\rangle\langle i,n,A|\mathrm{GS}\rangle \sum_{B,\sigma,\mu} (M^{\sigma,\mu}_{n,A;n-1,B})^2 \\
&\quad + \sum_{A'\neq A} \langle \mathrm{GS}|i,n,A'\rangle\langle i,n,A|\mathrm{GS}\rangle \\
&\quad \times \sum_{B,\sigma,\mu} M^{\sigma,\mu}_{n,A;n-1,B} M^{\sigma,\mu}_{n,A';n-1,B} \Bigg) \\
&= \sum_{n,A} p_{n,A} n, \qquad (35)
\end{aligned}
$$

in agreement with Eq. (32). In the third line of Eq. (35), use of the local orthonormality relations (5) was made. Note that the off-diagonal terms in Eq. (34) give no contribution to n_f due to the sum rules, Eq. (10), and independent of the approximation (29). The individual terms $np_{n,A}$ in the last sum of Eq. (35) arise from all local transitions $\Gamma=(n,A;n-1,B)$ with arbitrary B. The weight of all occupied states $|n-1,B\rangle$ in the one-particle f-excitation spectrum arising from local transitions from state $|n,A\rangle$ is exactly $np_{n,A}$. Since $p_{n,A}$ is the ground-state contribution of state $|n,A\rangle$ and therefore a ground-state property, the ground state uniquely and exactly reflects the integrated weight of occupied final states. The crucial step in the derivation of Eq. (35) is the implicit integration over energies of all occupied final states $|n-1,B\rangle$, which excludes information about the position of these states in energy. By integration, final-state mixing is *a priori* not addressed, which is a mixing of various final states at energies in the occupied part of the spectral density that are dominated by one final state. We note that within the approximations in this work mixing effects are small.

IV. SUMMARY AND CONCLUSIONS

The spectral density for SmS is determined using a multiband Anderson Hamiltonian. Emphasis is put on the high-energy one-particle and one-hole excitations up to 10 eV. The states are divided into localized, strictly nonitinerant $4f$ states, and delocalized band states c of s, p, and d character. The parameters for the band part are taken from a standard LDA calculation within the LCAO scheme[31] where six $4f$ states corresponding to divalent Sm^{2+} are put in the core. The $4f$ states form local many-electron states. 25 LS terms from $4f^4$ to $4f^7$ are taken into account together with corresponding transitions between LS terms that change the occupation number of the $4f$ shell by one. Spin-orbit splitting is neglected since it only leads to a fine structure in the excitation spectrum.

Next, the Hamiltonian is treated within a projection technique that is well suited to deal with local excitations. Two classes of dynamical variables are taken into account that contain the unhybridized limit exactly, and the effects of hybridization approximately. They form elementary excitations of the solid with a transparent interpretation. The next dynamical variables of type (25) that are neglected here should change the elementary excitations only in the low-energy region (0–0.3) eV near the chemical potential.

The semiconducting phase of SmS can be described with three parameters according to energy differences between local eigenstates of the $4f$ shell. The ^7F ground-state configu-

ration of f^6 representative for unhybridized $4f$ shells loses weight in favor of the ground-state configuration of f^5 and band states, dominated by Sm $5d$ states. Fair agreement is found between our calculated spectral density and experimental XPS data, while the BIS data are matched qualitatively. The $4f$ occupation of 5.94 in the semiconducting phase as found in this work is somewhat lower than the value >5.97 that was deduced from the experimental proportion of f^4/f^5 final-state weights in photoemission.[3] In light of our analysis, the contribution of f^4 final-state weight below 9.5 eV binding energy was underestimated in the experimental analysis.

An attempt has been made to simulate the mixed-valent phase by scaling the hybridization matrix elements. The scaling factor 2 used here for the golden phase is to be understood as an upper bound for the enlargement of the hybridization matrix elements due to the lattice contraction. Our hope was to model the experimental tendency for the change of the ground-state composition and the corresponding changes of final-state weights for the spectral density. We obtained a $4f$ occupation of 5.78 for the golden (contracted) phase. This value fits well to the value 5.77 ± 0.06 obtained from Vegard's law analysis of lattice constant measurements[35] and to that obtained from photoemission data (5.75, Ref. 3). It is higher, however, than the values of about 5.6 deduced from other spectroscopic methods like x-ray absorption at the L_{III} edge (5.57 ± 0.04, Ref. 34) and Mössbauer isomer shift (5.62 ± 0.08, Ref. 36). An unreasonable high scaling factor of about 5 would be needed to reproduce the latter values. We therefore conclude that our model is capable of describing the correct tendency; however, for a quantitative description either the approximations for the determination of the Green function are not accurate enough or the model itself is insufficient. In particular, hybridization enlargement is possibly not the only mechanism responsible for the valence transition in SmS. On the other hand, we would like to point to the obviously different $4f$ occupations found by different experimental techniques.

Calculated and experimental spectral densities for the mixed-valent phase agree reasonably well. However, this comparison is not free of ambiguity since the experiments were not carried out under pressure but using chemical modifications to prepare the mixed-valent phase. Because of the rather gross treatment of the excitation spectrum, our model is not suited to reproduce the insulator-to-metal transition connected with the mixed-valence transition of SmS.

From the experimental side, measurements of occupied and unoccupied states spectra on one and the same sample are still lacking. Such data could provide a safer basis for further theoretical investigations.

ACKNOWLEDGMENTS

We would like to thank P. Fulde for his suggestions and his encouragement, and R. Hayn, K. Koepernik, C. Laubschat, P. Thalmeier, and R. Schumann for various discussions.

APPENDIX A: SYMMETRY-REDUCED MATRIX ELEMENTS

In the following, the matrix elements $M_\Gamma^{\sigma,\mu}$ occurring in Eq. (8) will be reduced. We assume an underlying spherical symmetry although this would not *a priori* be necessary. However, a realistic point group does not make any difference because we sum in Eq. (27) over all single-ion, i.e., spherical degeneracies.

The transitions Γ take the form

$$\Gamma=(n,L,S,M_L,M_S;n-1,L',S',M_L',M_S'). \tag{A1}$$

The matrix elements $M_\Gamma^{\sigma,\mu}$ in spherical symmetry can be reduced according to the Wigner-Eckart theorem:[37,38]

$$\begin{aligned} M_\Gamma^{\sigma,\mu} &\overset{\mathrm{def}}{=} \langle n-1,L',S',M_L',M_S'|f^{l=3,\mu}_{s=1/2,\sigma}|n,L,S,M_S,M_L\rangle \\ &= (-1)^{L-M_L}\begin{pmatrix} L & l & L' \\ -M_L & \mu & M_{L'}\end{pmatrix} \\ &\quad\times(-1)^{S-M_S}\begin{pmatrix} S & s & S' \\ -M_S & \sigma & M_{S'}\end{pmatrix} \\ &\quad\times\left(n-1,L',S'\left\|f^{l=3}_{s=\frac{1}{2}}\right\|n,L,S\right). \end{aligned} \tag{A2}$$

Here, the terms in large parentheses denote the Wigner $3j$ symbol,[38] and $(\cdots\|\cdots\|\cdots)$ is a reduced matrix element. All reduced matrix elements that are used in this work are listed in Table II.

Summation over single-ion degeneracies gives

$$\sum_{M_{L'},M_{S'},M_L,M_S}(M_\Gamma^{\sigma,\mu})^2=(n-1,L',S'\|f_s^l\|n,L,S)^2\frac{1}{[l][s]}. \tag{A3}$$

Here, $[A]\equiv 2A+1$ stands for the number of basis functions associated with quantum number A. Use has been made of the closing relations for Wigner $3j$ symbols.[38] Therefore, one finds for the effective matrix elements defined in Eq. (27):

$$M^2_{\Gamma\ \mathrm{eff}}=(n-1,L',S'\|f_s^l\|n,L,S)^2\frac{1}{[l][s][L][S][L'][S']}. \tag{A4}$$

APPENDIX B: FREQUENCY AND SUSCEPTIBILITY MATRIX ELEMENTS

In the following, the frequency and susceptibility matrix elements in the space of the dynamical variables (23) and (24) are given. $\Gamma=(n,A;n-1,B)$, $\Delta=(m,C;m-1,D)$, and $\Lambda=(l,E;l-1,F)$ denote local transitions, n,m,l are occupation numbers, and A,B,C,D,E,F the quantum numbers LS of the $4f$ shell. A summation over free ion degeneracies M_L,M_S in Γ,Δ,Λ is assumed, according to Eq. (26). The multiplicity of quantum number A is abbreviated with $[A]=2A+1$. $\mathbf{k},\mathbf{q},\mathbf{p}$ are lattice momenta. α,β indicate orbital indices and σ,τ spin indices of the band basis states c. The

approximation (30) is used. $V^{\alpha,\Gamma}_{\mathbf{k},\sigma}$ has to be considered as the effective matrix element $(V^{\alpha,\Gamma}_{\mathbf{k}})^{\mathrm{eff}}$ of Eq. (28):

$$\chi^{\Delta,\Gamma}_{\mathbf{k},\mathbf{q}} \overset{\mathrm{def}}{=} \langle [(X^{\Delta}_{\mathbf{k}})^{\dagger}, X^{\Gamma}_{\mathbf{q}}]_{+} \rangle$$

$$= (\delta_{\mathbf{kq}} \delta_{\Delta\Gamma} [B] \langle |i,n,A\rangle\langle i,n,A| \rangle + [A] \langle |i,n-1,B\rangle\langle i,n-1,B| \rangle), \tag{B1}$$

$$F^{\Delta,\Gamma}_{\mathbf{k},\mathbf{q}} \overset{\mathrm{def}}{=} \langle [(X^{\Delta}_{\mathbf{k}})^{\dagger}, [H, X^{\Gamma}_{\mathbf{q}}]_{-}]_{+} \rangle$$

$$= \delta_{\mathbf{kq}} \delta_{\Gamma\Gamma} (E_{n-1,B} - E_{n,A}) \chi^{\Gamma,\Gamma}_{\mathbf{k},\mathbf{q}} - \delta_{\mathbf{kq}} \frac{1}{N_i} \sum_{\mathbf{p},\Lambda,\sigma,\alpha} (V^{\alpha,\Lambda}_{\mathbf{p},\sigma})^{*} \delta_{nl} e^{i\mathbf{p}\mathbf{R}_i}$$

$$\times (\delta_{BF}\delta_{DE}\delta_{m-1,l} \langle |i,n+1,C\rangle\langle i,n,A| c^{\alpha}_{\mathbf{p},\sigma} \rangle - \delta_{BF}\delta_{AC}\delta_{nm} [B] \langle |i,n,E\rangle\langle i,n-1,D| c^{\alpha}_{\mathbf{p},\sigma} \rangle + \delta_{AE}\delta_{DB}\delta_{nm} [A] \langle |i,n,C\rangle\langle i,n-1,F| c^{\alpha}_{\mathbf{p},\sigma} \rangle - \delta_{AE}\delta_{CF}\delta_{m,l-1} \langle |i,n-1,B\rangle\langle i,n-2,D| c^{\alpha}_{\mathbf{p},\sigma} \rangle), \tag{B2}$$

$$F^{\Gamma;\alpha,\sigma}_{\mathbf{k},\mathbf{q}} \overset{\mathrm{def}}{=} \langle [X^{\Gamma\dagger}_{\mathbf{k}}, [H, c_{\mathbf{q},\sigma}]_{-}]_{+} \rangle = -\delta_{\mathbf{kq}} \sum_{\Lambda} V^{\alpha,\Lambda}_{\mathbf{k},\sigma} \chi^{\Gamma,\Lambda}_{\mathbf{k},\mathbf{q}}, \tag{B3}$$

$$\chi^{\alpha,\sigma;\beta\tau}_{\mathbf{k},\mathbf{q}} \overset{\mathrm{def}}{=} \langle [c^{\alpha\dagger}_{\mathbf{k},\sigma}, c^{\beta}_{\mathbf{q},\tau}]_{+} \rangle = \delta_{\mathbf{kq}} \delta_{\sigma\tau} (\underline{\underline{O^{cc}_{\mathbf{k}}}})_{\alpha\beta}, \tag{B4}$$

$$F^{\alpha,\sigma;\beta,\tau}_{\mathbf{k},\mathbf{q}} \overset{\mathrm{def}}{=} \langle [c^{\alpha\dagger}_{\mathbf{k},\sigma}, [H, c^{\beta}_{\mathbf{q},\tau}]_{-}]_{+} \rangle = -\delta_{\mathbf{kq}} \delta_{\sigma\tau} (\underline{\underline{H^{cc}_{\mathbf{k}}}})_{\alpha\beta}. \tag{B5}$$

[1] C. M. Varma, Rev. Mod. Phys. **48**, 219 (1976).

[2] A. Jayaraman, V. Narayanamurti, E. Bucher, and R. G. Maines, Phys. Rev. Lett. **25**, 1430 (1970); A. Chatterjee, A. K. Singh, and A. Jayaraman, Phys. Rev. B **6**, 2285 (1972).

[3] M. Campagna, E. Bucher, G. K. Wertheim, and L. D. Longinotti, Phys. Rev. Lett. **33**, 165 (1974).

[4] H. L. Davis, *Proceedings of the 9th Rare Earth Conference, Blacksburg, 1971* (Elsevier, Amsterdam, 1977).

[5] O. V. Farberovich, Fiz. Tverd. Tela (Leningrad) **22**, 669 (1980) [Sov. Phys. Solid State **22**, 393 (1980)]; Phys. Status Solidi B **104**, 365 (1981).

[6] P. Strange, J. Phys. C **17**, 4273 (1984); Physica B & C **130**, 44 (1985).

[7] Z. W. Lu, D. J. Singh, and H. Krakauer, Phys. Rev. B **37**, 10 045 (1988).

[8] F. López-Aguilar and J. Costa-Quintana, J. Phys. C **19**, 2485 (1986); F. López-Aguilar, *ibid.* **19**, L735 (1986); S. Balle, J. Costa-Quintana, and F. López-Aguilar, Phys. Rev. B **37**, 6615 (1988).

[9] R. Schumann, M. Richter, L. Steinbeck, and H. Eschrig, Phys. Rev. B **52**, 8801 (1995).

[10] J. K. Lang, Y. Baer, and P. A. Cox, J. Phys. F **11**, 121 (1981).

[11] G. Borstel, Appl. Phys. A: Solids Surf. **38**, 193 (1985).

[12] H. G. Baumgärtel and E. Müller-Hartmann, in *Valence Instabilities*, edited by P. Wachter and H. Boppart (North-Holland, Amsterdam, 1982), p. 57.

[13] A. J. Fedro and S. K. Sinha, in *Valence Instabilities* (Ref. 12); A. J. Fedro and S. K. Sinha, *Moment Formation in Solids*, (Springer, Berlin, 1983), p. 135; A. J. Fedro and B. D. Dunlap, Jpn. J. Appl. Phys. Part 1 **26**, Suppl. 26-3, 463 (1987).

[14] T. Costi, J. Magn. Magn. Mater. **47&48**, 384 (1985).

[15] H. Kaga, H. Kubo, and T. Fujiwara, Phys. Rev. B **37**, 341 (1988).

[16] O. Sakai, S. Seki, and M. Tachiki, J. Phys. Soc. Jpn. **45**, 1465 (1978).

[17] R. M. Martin and J. W. Allen, J. Appl. Phys. **50**, 11 (1979).

[18] J. Leder and G. Czycholl, Z. Phys. B **35**, 7 (1979); G. Czycholl and H. J. Leder, *ibid.* **44**, 59 (1981); K. Elk, Phys. Status Solidi B **105**, 507 (1981); **107**, 387 (1981).

[19] Neglecting *f*-*c* overlap matrix elements is an important technical simplification.

[20] W. T. Carnall, P. R. Fields, and K. Rajnak, J. Chem. Phys. **49**, 4424 (1968); **49**, 4443 (1968); **49**, 4447 (1968); **49**, 4450 (1968); H. M. Crosswhite, R. L. Schwiesow and W. T. Carnall, *ibid.* **49**, 5032 (1968).

[21] J. Hubbard, Proc. R. Soc. London, Ser. A **277**, 237 (1964); **285**, 542 (1964).

[22] G. Racah, Phys. Rev. **76**, 1352 (1949).

[23] R. Zwanzig, *Lectures in Theoretical Physics* (Interscience, New York, 1961), Vol. 3.

[24] H. Mori, Prog. Theor. Phys. **33**, 423 (1965); **34**, 399 (1965).

[25] Laura M. Roth, Phys. Rev. Lett. **20**, 1431 (1968); Phys. Rev. **184**, 451 (1969).

[26] P. Fulde, *Electron Correlations in Molecules and Solids* (Springer, Berlin, 1997).

[27] P. Unger and P. Fulde, Phys. Rev. B **48**, 16 607 (1993).

[28] P. Unger, J. Igarashi, and P. Fulde, Phys. Rev. B **50**, 10 485 (1994).

[29] P. Unger and P. Fulde, Phys. Rev. B **51**, 9245 (1995).

[30] B. Mehlig, H. Eskes, R. Hayn, and M. B. J. Meinders, Phys. Rev. B **52**, 2463 (1995).

[31] H. Eschrig, *Optimized LCAO-Method and the Electronic Structure of Extended Systems* (Springer, Berlin, 1989).

[32] W. C. Martin, R. Zalubas, and L. Hagan, *Atomic Energy Levels—The Rare-Earth Elements*, Natl. Bur. Stand. Ref. Data Ser., Natl. Bur. Stand. (U.S.) Circ. No. 60 (U.S. GPO, Washington, D.C., 1978).

[33] S.-J. Oh and J. W. Allen, Phys. Rev. B **29**, 589 (1984).

[34] J. Röhler, in *Handbook on the Physics and Chemistry of Rare Earths*, edited by K. A. Gschneidner, Jr., L. Eyring, and S. Hüfner (North-Holland, Amsterdam, 1987), Vol. 10, Chap. 71.

[35] M. B. Maple and D. Wohlleben, Phys. Rev. Lett. **27**, 511 (1971).

[36] J. M. D. Coey, S. K. Ghatak, and F. Holtzberg, in *Proceedings of the 20th Annual Conference on Magnetism and Magnetic Materials, San Francisco, 1974* (American Instutute of Physics, New York, 1975); J. M. D. Coey, S. K. Ghatak, M. Avignon, and F. Holtzberg, Phys. Rev. B **14**, 3744 (1976).

[37] L. L. Hirst, Phys. Rev. B **15**, 1 (1977).

[38] A. R. Edmonds, *Angular Momentum in Quantum Mechanics* (Princeton University Press, Princeton, NJ, 1957).